Effect of Trifluoroethanol on a Tardigrade Desiccation-Tolerance Protein

By

Shikun ‘Rinco’ Wang

Senior Honors Thesis

Chemistry Department

University of North Carolina at Chapel Hill

April 25, 2022

Approved by:

Gary Pielak, Thesis Advisor

Sergei Sheiko, Committee Member

Anna Curtis, Committee Member

Abstract

Protein-based drugs revolutionized medicine, yet require a cold-chain, low temperature transport and storage. Dry formulations offer a room temperature alternative. Tardigrades, a phylum of microscopic animals capable of surviving complete desiccation, offer a promising route towards this goal. My project focuses on a particular tardigrade desiccation-tolerance protein, cytosolic abundant heat soluble (CAHS) D. CAHS D protects client proteins from inactivation *in vitro* but the mechanism is unknown. My graduate student mentor and I showed that pure CAHS D forms a concentration-dependent thermoreversible gel cross-linked by intermolecular β-sheets, and we posit the gel matrix acts as a molecular shield upon desiccation. Here, trifluoroethanol (TFE) was used to mimic the effect of dehydration on CAHS D. Circular dichroism spectropolarimeter data indicated that low concentrations of CAHS D gained α-helix in TFE. At higher CAHS D concentrations, the protein went through liquid, gel, aggregate and phases, the latter with liquid-gel phase separation at increasing % TFE. Using attenuated total internal reflectance Fourier transformation infrared spectroscopy, I showed that gelation was due to intermolecular interactions between β-strands, which are not significant enough at low CAHS D concentration. I suggest that only at high CAHS D concentration did TFE mimic water deficiency, strengthening CAHS D gelation to let it act like a 'molecular shield' against water deficient environment.

Introduction

Therapeutic proteins are promising candidates for clinical applications.[1] These protein-based drugs, while potent, require low temperature for storage and transport and cost a great deal of money. While lyophilization with excipients has promising potential in stabilizing some proteins, this effect is not generalizable.[2] In search of a general and effective stabilizer for dried proteins, we turn to tardigrades, a phylum of microscopic animals able to survive dehydration.

Research has shown that tardigrades upregulate the expressions of genes encoding three novel families of intrinsically disordered proteins, including cytosolic-, secreted-, and mitochondrial- abundant heat-soluble (CAHS, SAHS, MAHS) proteins, in response to desiccation.[3] RNA interference data demonstrates that these proteins are necessary for tardigrade's desiccation tolerance, while heterologous expression of them is sufficient to confer desiccation tolerance in both prokaryotic and eukaryotic cells.[4]

The protein CAHS D has been extensively studied in our lab. We have shown that CAHS D can protect lactate dehydrogenase (LDH) from desiccation-inactivation and globular protein GB1 (protein G, domain B1) from unfolding in the dried state.[5,6] Nevertheless, the molecular mechanism contributing to this protection is still under debate. We have demonstrated that pure CAHS D forms a concentration-dependent thermoreversible gel composed of coiled-coiled strands cross-linked with β-sheet. We hypothesized that this gel-matrix acts like a molecular shield to protect proteins from dehydration damage.

Other desiccation tolerance proteins (CAHS 1 & LEAM) at lower concentrations, under trifluoroethanol (TFE), which could mimic water deficiency, form α-helices but with no gelation reported.[7,8] It should be noted that sufficient levels of TFE will induce α-helices in most proteins, casting doubts on the relationship between α-helix and dehydration in CAHS D.[9] Moreover, while

β-sheet-contributed aggregation was reported in folded protein at medium % TFE, it was also not seen in desiccation-tolerance proteins.[7,8] Therefore, it is necessary to investigate effect of TFE on CAHS D at different concentrations to determine phase behavior and secondary structural shift under TFE-induced dehydration.

In this study, I used a range of biophysical tools to study CAHS D at different concentrations with TFE. Under increasing % TFE (v/v), I quantified CAHS D phase behavior and secondary structures with Circular Dichroism (CD) Spectroscopy at low concentration and with attenuated total internal reflectance Fourier transformation infrared (ATR-FTIR) Spectroscopy at high concentration. I also measured the amount of aggregation with UV-Vis Spectroscopy and FTIR. By measuring gel melting points through temperature curves, I characterized the forces strengthened under TFE. Investigating how TFE affects CAHS D helps shed light on how dehydration affects CAHS D at the scale of secondary structures. Collectively, these results lay the groundwork for understanding the molecular mechanism of CAHS D desiccation tolerance and contribute to its application as an excipient for therapeutics.

Results

α-helices induced at low CAHS D concentration under TFE

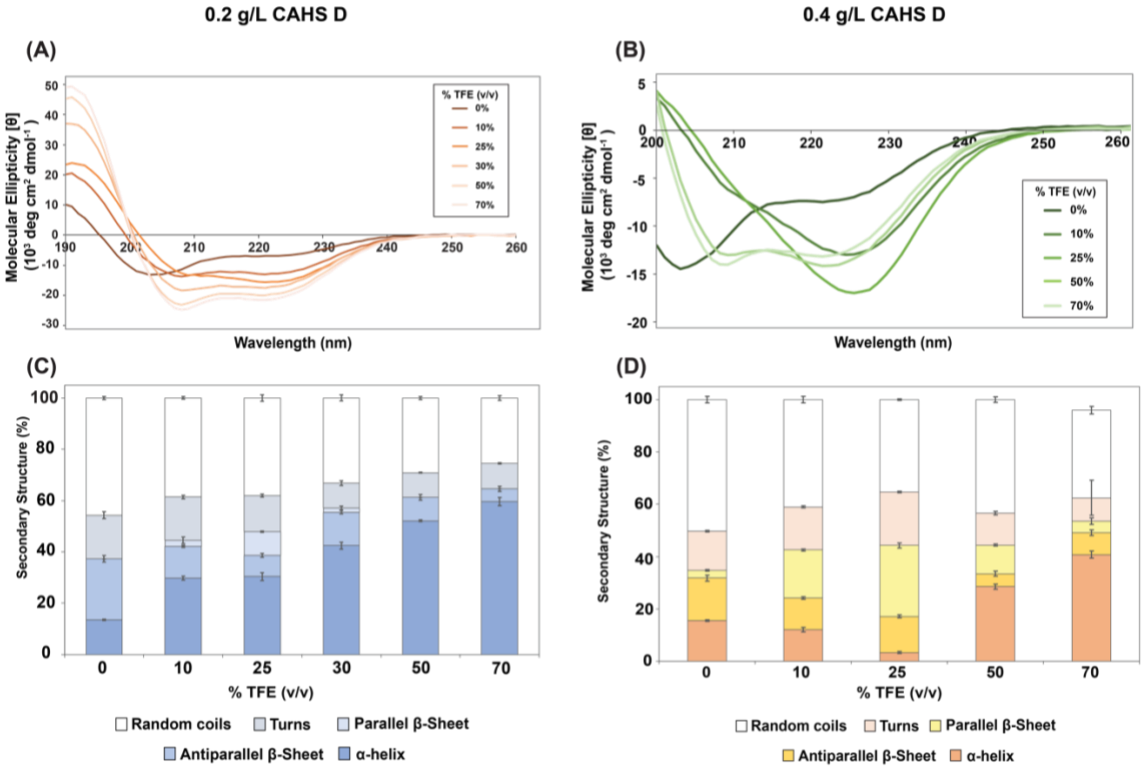

Figure 1. Effect of TFE on CAHS D at low concentrations (0.2 g/L & 0.4 g/L). (A)&(B): CD spectra of CAHS D in the absence and presence at different % TFE (v/v) at 0.2 g/L and 0.4 g/L, respectively. (C)&(D): Estimation of the secondary structure deduced from corresponding CD spectra using BeStSel program[10] at 0.2 g/L and 0.4 g/L CAHS D, respectively.

CD Spectroscopy was conducted at low CAHS D concentration to evaluate its secondary structure under TFE. As shown in **Figure 1A,** at 0.2 g/ L, CAHS D had a single negative minimum peak at around 200 nm without TFE, indicating that it is an unstructured protein in hydrated solution. As % TFE increased from 0 to 70, there was a significant shift towards typical α-helical structure, with two minima at 206 nm and 220 nm. Estimations of secondary structures **(Figure 1C)** agreed with the observations. As indicated, random coil predominated CAHS D secondary structures in solution, and the protein tended to fold into α-helices in the presence of increasing % TFE. This result agreed with the previously reported data in CAHS 1, and SAHS 1 protein, indicating that at low concentration CAHS D, α-helices were induced under TFE.[7]

Nevertheless, it should be noted that parallel β-Sheet was detected from 10% to 30% and reached maximum at 25%, which was not mentioned in past references. Spectra at 0.4 g/L CAHS D **(Figure 1B)** showed more significant change on parallel β-Sheet, with its proportion **(Figure 1D)** increased and reached maximum at 25% TFE and decreased from 50 to 70% TFE. Upon increasing % TFE, the protein at 0.4 g/L seemed to fold into β-Sheet first and then converted to α-helices.

At higher concentration (0.5-1.4 g/L), CAHS D exhibited different physical characteristics, with a viscous-gel state at 10 %, aggregation at 25 %, and solution at 50 %. It was impossible to determine the secondary structure at this concentration of CAHS D with CD Spectroscopy due to its high absorbance in the far-UV region. Furthermore, the aggregation displayed at 25 % TFE interfered with the measurement through light scattering.

The aggregation was quantified by measuring the scattering of light at 405 nm with UV-Vis Spectroscopy. As shown in **Figure 2**, absorbance at 25% TFE for all concentrations were generally higher, where aggregation was observed at 1.4 g/L, and parallel β-sheets were formed at 0.2 and 0.4 g/L CAHS D, demonstrating a possible relationship between parallel β-sheets and aggregation.

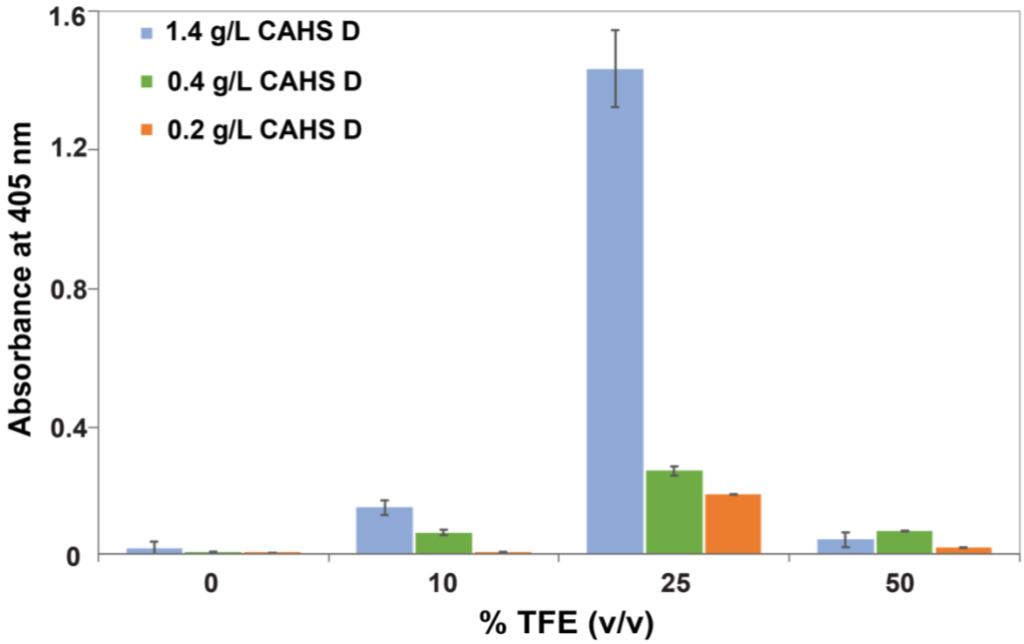

Figure 2. Aggregation of low concentration CAHS D under TFE. The extent of aggregation was measured by scattering of light at 405 nm across increasing % TFE (v/v) at 0.2, 0.4, and 1.4 g/L CAHS D, respectively.

β-sheet instead of α-helix contributed to TFE- induced gelation

At higher CAHS D concentration, more significant phase transitions were observed. As indicated in **Figure 3B**, when % TFE increased, CAHS D went through a gel, aggregates, liquid-gel phase separation transformation. The transition took place earlier as CAHS D concentration increased, demonstrating that the TFE-induced transition became more significant at higher concentration. When we mixed TFE and buffer first before diluting the protein, instead of a gel formed at bottom, we obtained aggregates.

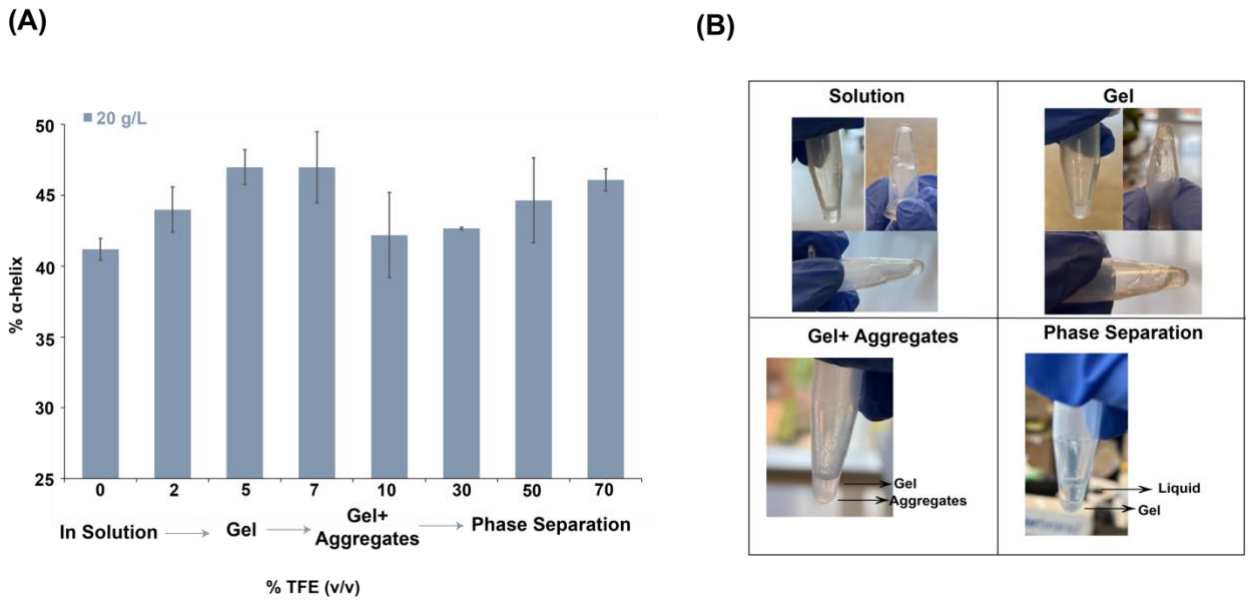

Figure 3. Structural and phase behavioral change of 20 g/L CAHS D under TFE. (A): % α-helix in the absence and presence of different % TFE (v/v), with the change of physical state indicated at the bottom. The gel phases were the ones measured at 30 %, 50%, and 70%. (B) Corresponding pictures of different physical states.

To quantify % α-helix, I obtained spectra from FTIR and performed peak fitting. Due to the low S/N ratio at 5 g/L and 10 g/L, I was only able to obtain reliable spectra and % α-helix at 20 g/L. **Figure 3A** showed that even though TFE induced gel formation at a low percentage, the proportion of α-helices was invariant to TFE, ranging from 40 % to 50 %. Moreover, if I took the uncertainties into consideration, the change was insignificant compared to the past research on other desiccation proteins, where they saw up to 70 % α-helix induced at 70 % TFE.[8] Therefore, TFE-induced gel was not likely due to α-helices.

To figure out if TFE induced intermolecular β-sheet that strengthened the gel, the gel melting point was measured using temperature curves. As shown in **Figure 4**, with 5 % TFE, the melting point increased from 300 K to 310.2 K, nearly the same as the one in 50 g/L (310 ± 2 K).

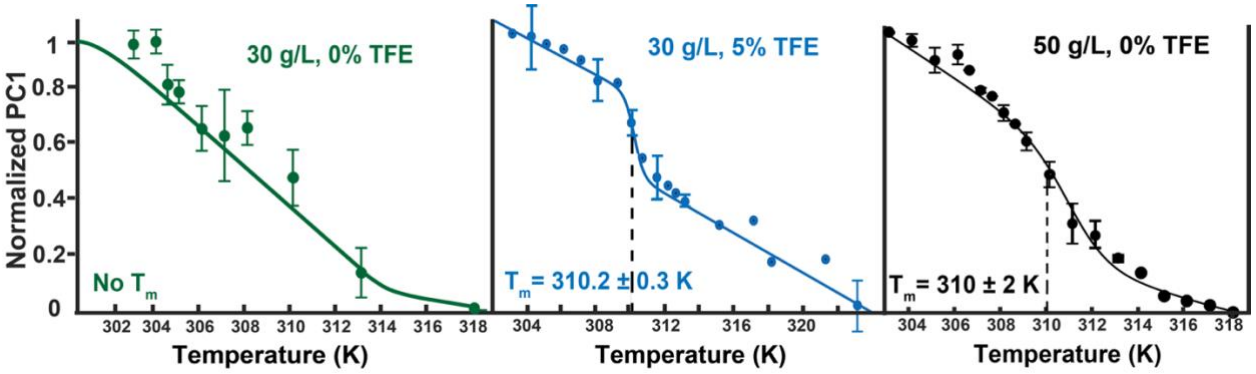

Figure 4. Gel melt curves of CAHS D. No T_m can be deducted at 30 g/L, 0 % TFE. The corresponding T_m were 310.2 ± 0.3 K at 30 g/L, 5% TFE, and 310 ± 2 K at 50 g/L, 0% TFE.

Considering the large uncertainties present in 30 g/L (0 %TFE), T_m was estimated from rheology (data unpublished) again in **Table 1**. The results of rheology agreed with the PC_1 data from FTIR, showing that T_m for 5 % TFE, 30 g/L CAHS D increased significantly with significant increase in % β-sheet while no significant change in % α-helix. Since low frequency β-sheets are more ordered and tended to form intermolecular interactions, and increasing melting point is also correlated with strengthening intermolecular forces, we concluded that the gel formed under 5 % TFE was likely due to intermolecular β-sheet formation.

CAHS D					
Concentration (g/L)	% TFE (v/v)	T_m(K) FTIR (PC1)	T_m(K) Rheology	% α-helix	% Low Frequency β-Sheet
30 g/L	0	300 ± 100	303.3 ± 0.9	46±1	34.2 ± 0.7
30 g/L	5	310.2 ± 0.3	N/A	44±2	38.9 ± 0.5
50 g/L	0	310 ± 2	309.89 ± 0.07	45.51 ± 0.04	39.3 ± 0.2

Table 1. Effect of TFE on CAHS D at high concentrations. Comparison of Tm, % α-helix and low frequency β-sheet at 30 °C with and without TFE of CAHS D at 30 g/L (0 % TFE), 50 g/L (0 % TFE) and 30 g/L (5% TFE) using FTIR and Rheology.

CAHS D Gel rejects further aggregation under high % TFE

The aggregation was quantified with FTIR using the average intensity of the secondary derivatives spectra at 1620 nm (β-sheet). As shown in **Figure 5**, aggregation increased from 0 % to 10 % TFE, and decreased at higher % TFE, when CAHS D went through the transformation from gel-aggregates to liquid-gel phase separation.

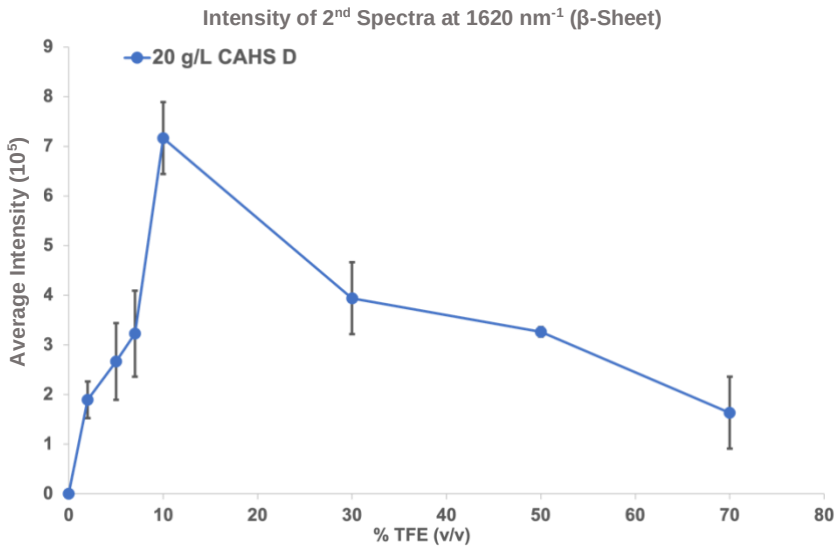

Figure 5. Aggregation of high concentration CAHS D under TFE. Average Intensity Secondary Derivatives Spectra at 1620 nm of CAHS D (20 g/L) in the absence and presence of different % TFE (v/v). The gel phases were the ones measured at 30 %, 50%, and 70%.

Figure 6A indicates the difference between the FTIR (only subtracted with background) of liquid top and gel bottom for CAHS D under 70% TFE in the Amide I+II region. Since H_2O only absorbs IR light at Amide I region, Amide II could be used as an indication of the protein presence. There was a peak in

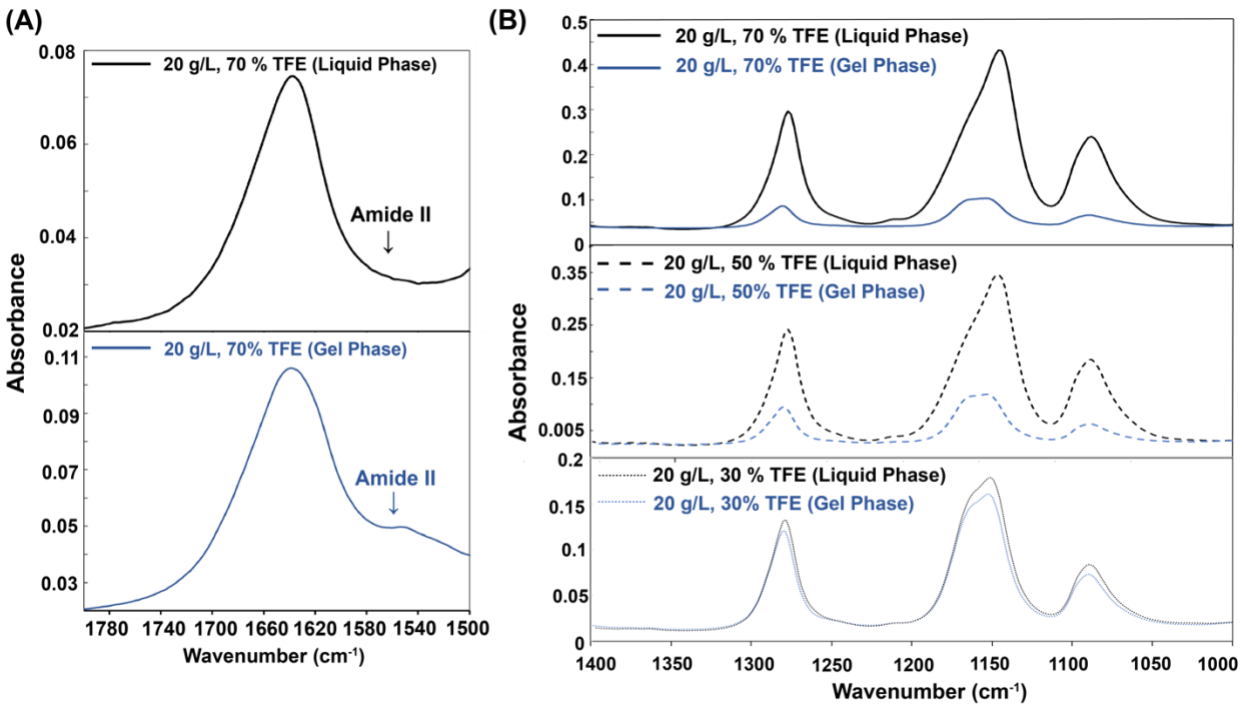

Figure 6. Unsubtracted FTIR spectra of the liquid and gel phase at 20 g/L CAHS D. (A): Stack spectra for two phases on Amide I and Amide II region (1500-1800 cm-1) for 20 g/L CAHS D at 70% TFE (B): Stack spectra for two phases in the TFE-specific region (1000-1400 cm^{-1}) for 20 g/L CAHS D at 30%, 50%, and 70% TFE respectively.

the gel spectrum of the Amide II region while there was no peak observed in the same region for the liquid spectrum. Plus, the absorbance of the Amide II region was significantly higher in the gel phase, demonstrating that most of the protein concentrated in the gel bottom. **Figure 6B** indicates that by identifying the TFE-characteristic peak in 1000-1400 cm^{-1}, TFE concentrated in the liquid phase at 30, 50, and 70% TFE. Thus, it seems at high % TFE, only part of the TFE was present in the protein rich phase, which formed a gel with nearly no aggregation observed. I quantified the % TFE in the protein rich phase with **Eq.1**. The results were concluded in **Figure 7**, demonstrating that while % TFE was similar between what was originally added and what was in the gel bottom phase when there was no phase separation; when there was a liquid-gel phase separation, no matter

$$\%\ \text{TFE in Gel Bottom Phase} = \frac{V(total\ TFE) * \frac{area\ of\ solid\ bottom}{area\ of\ solid\ bottom + area\ of\ liquid\ top}}{V(gel\ bottom)} \qquad \textbf{Eq. 1}$$

how much % TFE was added, there was only about 26.8 ± 0.9 % TFE in the gel phase, which was exactly at the transition stage when CAHS D went from aggregates to liquid-gel phase separation.

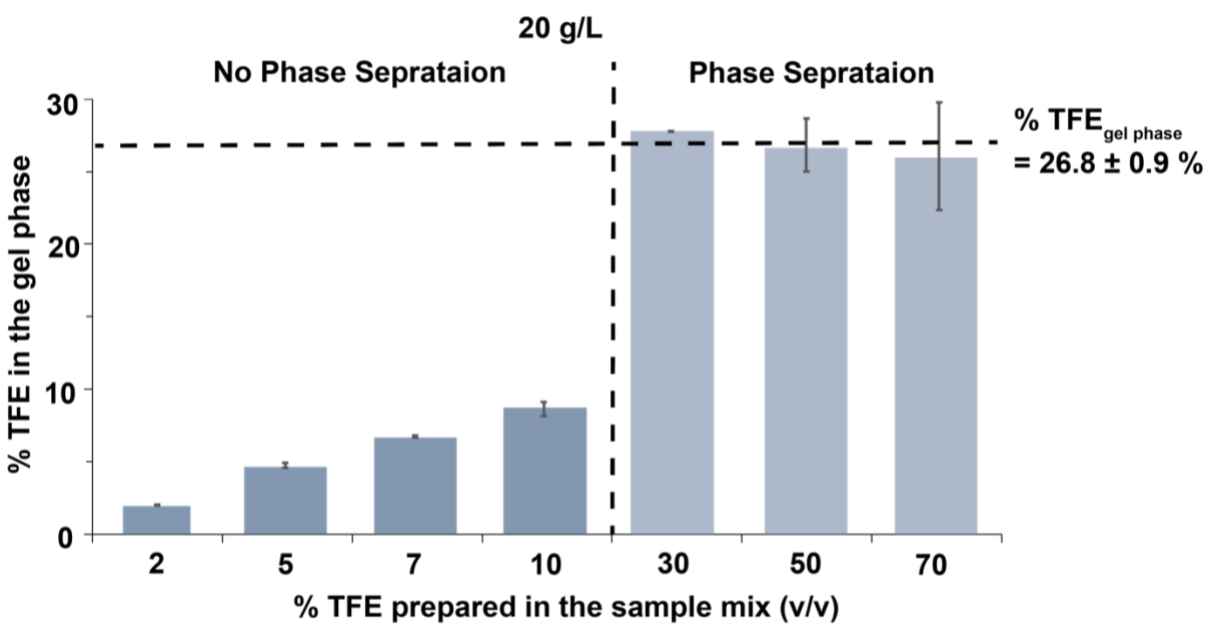

Figure 7. % TFE in CAHS D (20 g/L) with and without phase separation. When there was no phase separation, % TFE in the gel phase ≈ % TFE prepared in the sample mix. When there was a phase separation, % TFE in the gel phase = 26.8 ± 0.9 % as % TFE prepared in the sample mix = 30%, 50%, 70%.

Discussion

In this project, I investigated the effect of TFE, a desolvant mimicking dehydration, on CAHS D phase behavior and structural change at different protein concentrations. The results were concluded in a phase diagram of CAHS D concentration vs v/v TFE **(Figure 8)**.

At extremely low CAHS D concentrations (0.2 and 0.4 g/L), no gelation or aggregation was observed. The CD spectroscopy saw a significant shift towards α-helix under high % TFE at both 0.2 g/L and 0.4 g/L **(Figure 1 A&B)**. This result agreed with past TFE research on other desiccation proteins, including SAHS 1, CAHS 1, and Mitochondrial Late Embryogenesis Abundant Protein (LEAM), with their concentrations slightly higher (1 – 2 g/L).[7,8] At first glance,

it seems that CAHS D would go through a structural shift from random coils to α-helix upon desiccation. However, it should be noted that α-helices could also be induced in most protein with high % TFE.[9,11]Thus, a relationship between desiccation tolerance and structural shift to α-helix in CAHS D cannot be drawn.

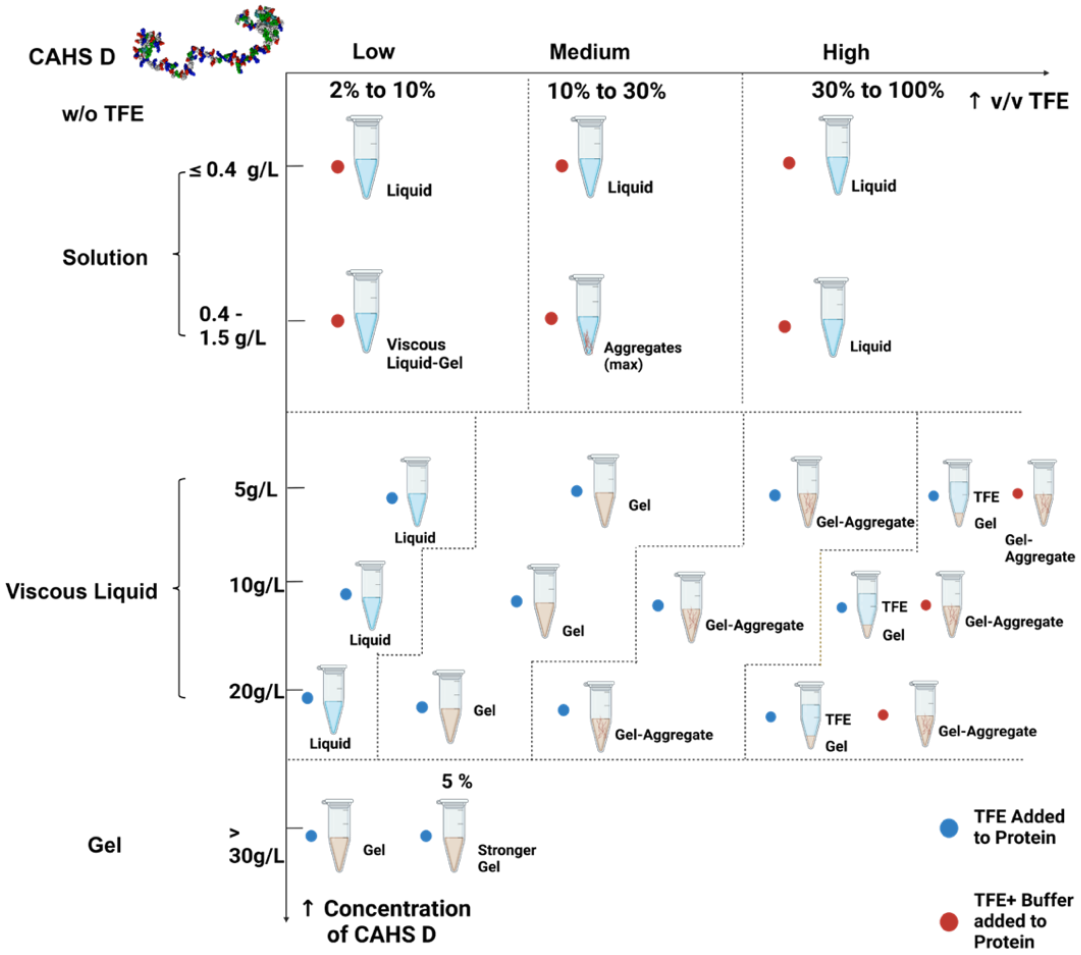

Figure 8. Phase behavior diagram of concentration vs. v/v TFE in CAHS D. Physical states and order of addition were annotated besides each Eppendorf tube. Created with Biorender.com

When I conducted similar experiments at 1.4 g/L, gel and aggregates were observed. The aggregation process was quantified using the scattering of light at 405 nm with UV-Vis Spectroscopy **(Figure 2)**. The absorbance reached maximum at 25% TFE, under which significant aggregation was observed. Similar aggregation processes were observed in native folded protein under the effect of TFE, in which the researchers hypothesized was caused by intermolecular β-

sheet formation.[11] However, only CAHS D showed gel formation at low % TFE. It should be noted that parallel β-sheets also reached maximum for lower CAHS D concentration (0.2 and 0.4 g/L) **(Figure 1 C&D)** at 25 % TFE, with β-sheet's proportion increasing at increasing concentration. Intermolecular parallel β-sheets have been previously observed in insoluble amyloid fibrillar aggregates related to Alzheimer, Parkinson, Huntington, and prion diseases.[12] Therefore, at low concentration CAHS D, the protein seemed to fold into parallel β-sheet under low % TFE and then transform into α-helix at high % TFE. If the CAHS D concentration was higher (1.4 g/L), even though secondary structure was unable to be derived at this concentration, it is likely the same process happened, and the observed aggregation was due to intermolecular parallel β-sheet interactions.

At higher CAHS D concentrations (> 5 g/L), both gel and aggregates can be measured with ATR-FTIR. Gel, aggregates, liquid-gel phase separation transition **(Figure 3B)** was observed under increasing %TFE, with the process occurring earlier as concentration increased, indicating TFE induced gel formation in CAHS D. However, there was no structural shift towards α-helix under higher % TFE, demonstrating that there was possibly no correlation between desiccation tolerance in CAHS D and α-helix **(Figure 3A).** The gel melting curves demonstrated a significant increase in the melting point in TFE-induced gel. **(Figure 4)** Since the melting process required the breaking of intermolecular interactions and considering the nature of aggregates in the gel-aggregates (β-sheet), the gel was likely to consist of intermolecular β-sheet. Deconvolution of FTIR spectra showed a significant increase in low frequency β-sheet while no significant change in α-helix in upon addition of TFE **(Table 1)**, proving the TFE-induced gel was indeed contributed by β-sheet.

The aggregation process at 20 g/L **(Figure 5**) also demonstrates that the force making the gel and aggregates should be the same. Increasing % TFE increased the strength of the force, turning CAHS D from liquid, to gel, and thus to aggregates. The analysis of the liquid top and gel bottom phase at even higher % TFE **(Figure 6**), on the other hand, indicated a transformation from aggregation back to gel state. Quantifications of TFE peak areas showed that (**Figure 7)** at high % TFE, CAHS D could take 26.8 ± 0.9 % TFE to make a gel and reject the rest. Considering dehydration process, this showed that CAHS D could sense the water availability and act against desiccation in the surroundings through gelation. Further research needs to be done to clarify why mixing TFE and buffer first would result in aggregation. But I hypothesize that mixing decreases %TFE to an extent that it could not induce phase separation.

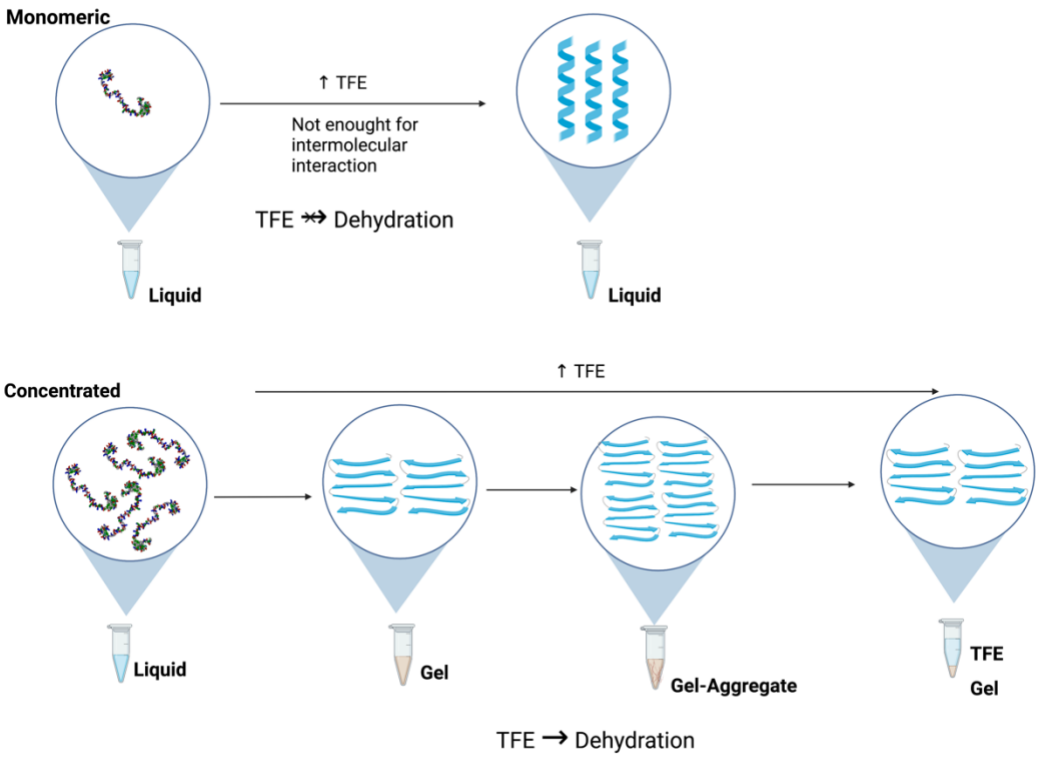

Figure 9. Monomeric and concentrated CAHS D structural and phase behavioral changes under increasing % TFE. Created with Biorender.com.

The detailed secondary structure changes behind CAHS D phase behaviors were concluded in **Figure 9.** When CAHS D concentration was low, the protein was nearly monomeric, making the intermolecular interaction not strong enough to form a gel. Therefore, even though parallel β-sheet was formed and led to aggregation at medium % TFE at slightly higher concentration of

CAHS D, interactions between β-sheets were too weak to persist that as TFE continuously increased, CAHS D acted like folded protein and shifted to α-helix. Under this condition, TFE was not a good desiccation mimicking agent. At higher concentration, TFE mimicked water deficiency. The intermolecular interaction between ordered low frequency β-sheets induced by TFE was strong enough to form a gel. As the interaction became stronger, part of the gel crashed into aggregates. Nevertheless, at extreme condition, CAHS D would protect itself against water deficiency, forming a gel that rejected further aggregation.

Conclusion

In this project, I clarified CAHS D phase behavior and structural changes at different protein concentrations under increasing level of TFE, which was commonly used to mimic water deficient conditions. While low concentration CAHS D responded like folded protein to form α-helix and TFE may not be a good mimicking agent, at higher concentration, TFE mimicked the dehydration process, inducing the intermolecular interactions between β-sheet to strengthen the gelation. Instead of crashing into aggregates like folded proteins, CAHS D was able to resist further aggregation and kept itself at a stable gel state.

CAHS D's ability to form an exclusive gel under dehydration shed light on its molecular mechanism of desiccation tolerance, supporting the hypothesis that it acts as a molecular shield during desiccation through its gel structure by stabilizing the local environment of the gel. Nevertheless, it remains unclear how this gel structure exactly contributed to desiccation tolerance at the molecular level. Further research could be focused on figuring out the detailed mechanism. I could also conduct the experiments on dry-state CAHS D, which could serve as a good comparison with the dehydrated ones under TFE. Moreover, investigating CAHS D secondary

structure under a variety of conditions, such as pH and ionic strength, would be important in understanding its gel structure.

Understanding CAHS D structural and phase behavior change under dehydration clarifies how this desiccation-tolerance protein helps tardigrade and other proteins remain stable under desiccation. Together, these results shed light on CAHS D's ability as a promising excipient for protein-based drugs.

Material and Methods

CAHS D Purification

Expression and purification of CAHS D was carried out as described.[13] To summarize, CAHS D-His pET28-b plasmid was transformed into BL21 (DE3) cell. The cultures were incubated with shacking at 37 °C until the optical density at 600 nm reached 0.6 (BioRad SmartSpec Plus spectrophotometer) and induced with isopropyl β- d-1-thiogalactopyranoside (IPTG) (1 mM final concentration) for 3 hours. After centrifuge, the pellet was resuspended in 5 mL 20 mM Tris buffer (pH 7.4) and stored under -20 °C.

For purification, the frozen cell pellets were thawed in water batch and then lysed by heat-shock. The samples were centrifuged again, diluted using equal volumes of HU_A (3M Urea, 20 mM $NaPO_4$, 500 mM NaCl, 10 mM imidazole, pH 7.4) and filtered with a 0.45 μm syringe filter (Millipore SLGVM33RS).

Samples were loaded to a His-Trap HP column (Thermo Fischer) and eluted at a linear gradient of imidazole from 0 % to 100 % for 30 fractions on a Fast protein liquid chromatography (FPLC) (ÄKTA™ Start). SDS-PAGE (Bio-Rad 4-20% Criterion™ TGX™ Gels) was used to determine the purity of fractions, which were dialyzed against 1X TEV digest buffer (5 mM Tris, 0.5 mM EDTA, pH 7.4). Samples were added with TEV (Tobacco Etch Virus) protease and dithiothreitol (DTT), incubated overnight to cleave the His tag, followed with the His-Trap HP column to collect flowthrough. The proteins were then dialyzed against 5 L 1XPBS (137 mM, 2.7 mM KCl, 8 mM Na_2HPO_4 pH 7.4) and 5 L H_2O until the total concentration of buffer was less than 1 nM.

Samples were flash frozen in a dry ice/ethanol bath and lyophilized (Labconco FreeZone) until all water is removed. Lyophilized CAHS D was resuspended in 1XPBS and quantified with

Pierce Coomassie Plus assay using a bovine serum albumin standard (Thermo Fisher) in 96-well plates.[14]

UV-Vis Spectroscopy

Aggregation of CAHS D was quantified by a UV-Vis Spectrophotometer (BioRad SmartSpec Plus spectrophotometer) by measuring the light scattering at 405 nm. The final concentration of CAHS D was diluted to 0.2 g/L, 0.4 g/L and 1.4 g/L, separately, with % TFE (v/v) set to 0, 10, 25, and 50. TFE was mixed with 1XPBS before added to the sample. Incubation time was set at 30 min for equilibration.

CD Spectroscopy

CD Spectra were obtained for CAHS D at low concentrations (less than 2 g/L) in the far-UV region (280 nm- 185 nm) on the Chirascan™-Plus (Applied Photophysics) Circular Dichroism Spectrophotometer, with the ambient temperature set at 30 °C. Lyophilized CAHS D was dissolved in 10 mM phosphate buffer (6.1 mMNa_2HPO_4, 3.9 mM NaH_2PO4, pH 7.4) instead of 1XPBS to exclude the interference of Cl^- absorbance in the far UV region. The final concentration of CAHS D was diluted to 0.2, 0.4 and 1.4 g/L, with % TFE (v/v) set to 0, 10, 25, 30, 50, and 70. TFE was mixed with 10 mM phosphate buffer before added to the sample. Incubation time was set at 30 min for proper mix. The results were reported in molar ellipticity, $[\theta] = \frac{m^\circ * M}{10 * L * c}$ degree cm^2 $dmol^{-1}$, where c is the concentration of the protein in g/L, L is the pathlength of the cell (0.1 cm), M is the mean residual weight of the protein in g/mol (112.27 g/mol).[15] Estimation of the secondary structures were done using the Beta Structure Selection (BEStSel) program.[10]

FTIR Spectroscopy

FTIR Spectra were obtained for CAHS D at higher concentration (higher than 5 g/L) on a Prota-3S FT-IR Spectrophotometer (Biotools), with the ambient temperature at 30 °C, the

wavenumber resolution of 4 cm^{-1}, and 400 scans. After redissolved in 1XPBS, CAHS D was quantified and diluted to 5, 10, and 20 g/L, with % TFE (v/v) as 0, 2, 5, 7, 10, 25, 50, and 70. TFE was either added last to the sample or mixed with 1XPBS before the dilution, followed with 30 min incubation time for proper mix. All spectra were processed and deconvoluted using Orange Data mining,[16] with the peaks assigned to different secondary structures according to literature values.[17] For the temperature scan, CAHS D was diluted to 30, 40, and 50 g/L, with % TFE (v/v) as 0 and 5. The procedures were similar, except for the scan number at 100, and ambient temperature at 30, 31, 32, 33, 34, 35, 36, 37, 37.5, 38, 38.5, 39, 40, 42, 44, 46, 48, 50 °C, separately. Principal Component Analysis (PCA) was conducted on the dataset of the gel melt experiment. Temperature curve was obtained from plotting PC1, the largest possible explained variation, against temperature and fitted to the two-state Gibbs-Helmholtz equation to get melting point Tm.[18]

Reference

1. Lagassé, H. A. D.; Alexaki, A.; Simhadri, V. L.; Katagiri, N. H.; Jankowski, W.; Sauna, Z. E.; Kimchi-Sarfaty, C. Recent Advances in (Therapeutic Protein) Drug Development. *F1000Res* **2017**, *6*, 113. https://doi.org/10.12688/f1000research.9970.1.
2. Merivaara, A.; Zini, J.; Koivunotko, E.; Valkonen, S.; Korhonen, O.; Fernandes, F. M.; Yliperttula, M. Preservation of Biomaterials and Cells by Freeze-Drying: Change of Paradigm. *Journal of Controlled Release* **2021**, *336*, 480–498. https://doi.org/10.1016/j.jconrel.2021.06.042.
3. Yamaguchi, A.; Tanaka, S.; Yamaguchi, S.; Kuwahara, H.; Takamura, C.; Imajoh-Ohmi, S.; Horikawa, D. D.; Toyoda, A.; Katayama, T.; Arakawa, K.; Fujiyama, A.; Kubo, T.; Kunieda, T. Two Novel Heat-Soluble Protein Families Abundantly Expressed in an Anhydrobiotic Tardigrade. *PLoS One* **2012**, *7* (8), e44209. http://dx.doi.org/10.1371/journal.pone.0044209.
4. Boothby, T. C.; Tapia, H.; Brozena, A. H.; Piszkiewicz, S.; Smith, A. E.; Giovannini, I.; Rebecchi, L.; Pielak, G. J.; Koshland, D.; Goldstein, B. Tardigrades Use Intrinsically Disordered Proteins to Survive Desiccation. *Mol Cell* **2017**, *65* (6), 975-984.e5. https://doi.org/10.1016/j.molcel.2017.02.018.
5. Piszkiewicz, S.; Mehta, A.; Boothby, T.; Daniel,der W.; Sheiko, S.; Goldstein, B.; Pielak, G. Tardigrade Intrinsically Disordered Proteins as Potential Excipients for Biologics. *Biophysical Journal* **2017**, *112*, 512a. https://doi.org/10.1016/j.bpj.2016.11.2766.
6. Crilly, C. J.; Brom, J. A.; Warmuth, O.; Esterly, H. J.; Pielak, G. J. Protection by Desiccation-Tolerance Proteins Probed at the Residue Level. *Protein Science* **2022**, *31* (2), 396–406. https://doi.org/10.1002/pro.4231.
7. Yamaguchi, A.; Tanaka, S.; Yamaguchi, S.; Kuwahara, H.; Takamura, C.; Imajoh-Ohmi, S.; Horikawa, D. D.; Toyoda, A.; Katayama, T.; Arakawa, K.; Fujiyama, A.; Kubo, T.; Kunieda, T. Two Novel Heat-Soluble Protein Families Abundantly Expressed in an Anhydrobiotic Tardigrade. *PLoS One* **2012**, *7* (8), e44209. http://dx.doi.org/10.1371/journal.pone.0044209.
8. Tolleter, D.; Jaquinod, M.; Mangavel, C.; Passirani, C.; Saulnier, P.; Manon, S.; Teyssier, E.; Payet, N.; Avelange-Macherel, M.-H.; Macherel, D. Structure and Function of a Mitochondrial Late Embryogenesis Abundant Protein Are Revealed by Desiccation. *Plant Cell* **2007**, *19* (5), 1580–1589. https://doi.org/10.1105/tpc.107.050104.
9. Ataei, F.; Hosseinkhani, S. Impact of Trifluoroethanol-Induced Structural Changes on Luciferase Cleavage Sites. *Journal of Photochemistry and Photobiology B: Biology* **2015**, *144*, 1–7. https://doi.org/10.1016/j.jphotobiol.2015.01.008.
10. Micsonai, A.; Wien, F.; Kernya, L.; Lee, Y.-H.; Goto, Y.; Réfrégiers, M.; Kardos, J. Accurate Secondary Structure Prediction and Fold Recognition for Circular Dichroism Spectroscopy. *Proc Natl Acad Sci U S A* **2015**, *112* (24), E3095–E3103. https://doi.org/10.1073/pnas.1500851112.
11. Srisailam, S.; Kumar, T. K. S.; Srimathi, T.; Yu, C. Influence of Backbone Conformation on Protein Aggregation. *J. Am. Chem. Soc.* **2002**, *124* (9), 1884–1888. https://doi.org/10.1021/ja012070r.
12. Benzinger, T. L. S.; Gregory, D. M.; Burkoth, T. S.; Miller-Auer, H.; Lynn, D. G.; Botto, R. E.; Meredith, S. C. Propagating Structure of Alzheimer's β-Amyloid (10–35)

Is Parallel β-Sheet with Residues in Exact Register. *Proc Natl Acad Sci U S A* **1998**, *95* (23), 13407–13412.
13. Esterly, H. J.; Crilly, C. J.; Piszkiewicz, S.; Shovlin, D. J.; Pielak, G. J.; Christian, B. E. Toxicity and Immunogenicity of a Tardigrade Cytosolic Abundant Heat Soluble Protein in Mice. *Front Pharmacol* **2020**, *11*, 565969. https://doi.org/10.3389/fphar.2020.565969.
14. M. M. Bradford, *Anal. Biochem.* **1976**, *72*, 248-254.
15. Purdie, N. Circular Dichroism and the Conformational Analysis of Biomolecules Edited by Gerald D. Fasman (Brandeis University). Plenum Press: New York. 1996. x + 738 Pp. $125.00. ISBN 0-306-45142-5. *J. Am. Chem. Soc.* **1996**, *118* (50), 12871–12871. https://doi.org/10.1021/ja965689f.
16. Yang, H.; Yang, S.; Kong, J.; Dong, A.; Yu, S. Obtaining Information about Protein Secondary Structures in Aqueous Solution Using Fourier Transform IR Spectroscopy. *Nat Protoc* **2015**, *10* (3), 382–396. https://doi.org/10.1038/nprot.2015.024.
17. Demsar J, Curk T, Erjavec A, Gorup C, Hocevar T, Milutinovic M, Mozina M, Polajnar M, Toplak M, Staric A, Stajdohar M, Umek L, Zagar L, Zbontar J, Zitnik M, Zupan B (2013) Orange: Data Mining Toolbox in Python, *Journal of Machine Learning Research* 14(Aug): 2349−2353.
18. Cohen, D. S.; Pielak, G. J. Stability of Yeast Iso-1-Ferricytochrome c as a Function of PH and Temperature. *Protein Sci* **1994**, *3* (8), 1253–1260.